Geophysical Research Letters

RESEARCH LETTER
10.1029/2025GL120069

The "Predictability Barrier" Phenomenon of Winter Extreme Cold Events in Central and Eastern China and Mechanisms of Error Amplification

Zhe Han[1,2], Wansuo Duan[3], Guokun Dai[2], Shuanglin Li[4], Boyu Chen[5], and Yuxuan Hou[3]

[1]Laboratory of Regional Climate-Environment for Temperate East Asia, Institute of Atmospheric Physics, Chinese Academy of Sciences, Beijing, China, [2]Shanghai Key Laboratory of Ocean-land-atmosphere Boundary Dynamics and Climate Change, Department of Atmospheric and Oceanic Sciences & Institute of Atmospheric Sciences, Fudan University, Shanghai, China, [3]State Key Laboratory of Earth System Numerical Modeling and Application, Institute of Atmospheric Physics, Chinese Academy of Sciences, Beijing, China, [4]Climate Change Research Center, Institute of Atmospheric Physics, Chinese Academy of Sciences, Beijing, China, [5]National Meteorological Center, China Meteorological Administration, Beijing, China

Abstract Previous studies have primarily focused on evaluating the forecast skill of extreme cold events in central and eastern China as a whole, with limited attention to their different stages. This study identifies a distinct "predictability barrier" phenomenon in the ensemble forecasts, characterized by rapid growth of ensemble mean forecast error in 2m-temperature during the intensification stage of the events. In contrast, the forecast error tends to decrease during the decay stage. Consequently, the decay stage is more accurately forecasted than the intensification stage at the same lead time. Mechanism analyses indicate that error amplification is primarily driven by the interaction between the horizontal wind forecast error and the background horizontal temperature gradient of the event, which is dominantly governed by event intensification. Error reduction during the decay stage is primarily dominated by the conversion of available potential energy error into kinetic energy error.

Plain Language Summary Previous research indicates that extreme cold events can generally be forecast accurately with a lead time of about 7 days. This study finds that the main challenge of forecasting at longer lead times arises from the rapid growth of forecast errors during the intensification stage of events, referred to as the "predictability barrier." Unlike the rapid error growth during the intensification stage, the forecast error tends to decrease during the decay stage. This means that the forecast skill during the decay stage is better than during the intensification stage for the same lead time. Mechanism analyses demonstrate that the physical processes governing event intensification play a crucial role in the occurrence of the "predictability barrier." Meanwhile, the conversion between available potential energy error and kinetic energy error inhibits the occurrence of the "predictability barrier."

Key Points:

- A distinct "predictability barrier" phenomenon is identified during the intensification stage of cold events
- The forecast error tends to grow rapidly during the intensification stage, while decreasing during the decay stage
- Physical processes governing event intensification are responsible for error amplification

Supporting Information:

Supporting Information may be found in the online version of this article.

Correspondence to:

W. Duan and G. Dai,
duanws@lasg.iap.ac.cn;
daigk@fudan.edu.cn

Citation:

Han, Z., Duan, W., Dai, G., Li, S., Chen, B., & Hou, Y. (2026). The "predictability barrier" phenomenon of winter extreme cold events in central and eastern China and mechanisms of error amplification. *Geophysical Research Letters*, *53*, e2025GL120069. https://doi.org/10.1029/2025GL120069

Received 4 NOV 2025
Accepted 26 FEB 2026

1. Introduction

Despite the ongoing global warming, extreme cold events in winter still occur in China from time to time. For instance, nine extreme cold events took place over the past decade, with the surface air temperature even breaking the record in several events. One notable example is the extreme cold event during 20–25 January 2016, often referred to as the "boss level" cold wave, which attacked many regions of China. During this event, the surface air temperature in East Asia reached the historical record low (Ma & Zhu, 2019; Song & Wu, 2017). Two years later, an extreme event hit most of China during 24–28 January 2018 (Dong et al., 2020; Huang et al., 2022; Liu et al., 2018). Additionally, a nationwide extreme cold event occurred during 25–31 December of the same year (Dai et al., 2021). During the 2020/2021 winter, three successive extreme cold events affected eastern China, with many stations reporting record low temperatures (Yao et al., 2022; Zhang et al., 2022; Zheng et al., 2022). Similarly, during the 2023/2024 winter, three extreme cold events hit China, posing significant challenges to the Spring Festival travel rush (Chen et al., 2024; Gong et al., 2024; Ye et al., 2025). The extreme cold event is a type of high-impact weather that is often accompanied by secondary disasters, such as freezing rain and heavy snowfall, and leads to severe disruptions in transportation, energy supply, agriculture, and livestock husbandry. Consequently, research on the predictability of extreme cold events is of great importance for disaster prevention and mitigation strategies.

Many studies have assessed the forecast skill of extreme cold events in China. For example, studies on the extreme cold events in January 2008 indicate that the events cannot be accurately predicted beyond 5 days in advance, based on analysis of the extreme forecast index (EFI) (Xia & Chen, 2012). The EFI, developed by the European Centre for Medium-Range Weather Forecasts (ECMWF), is an effective index for identifying extreme weather events (Lalaurette, 2003; Zsoter, 2006). Similar findings have been reported in studies using alternative metrics, where forecast errors grow substantially at lead times longer than 5 days (Zhang et al., 2021; Zheng et al., 2020). Based on EFI analyses, extreme cold event in late January 2016, as well as those in January and December 2018, can be accurately predicted up to 7 days in advance (Dai et al., 2021; Tao et al., 2017). Furthermore, predictions of three consecutive extreme cold events during the 2020/2021 winter indicate that they can be skillfully forecast with a lead time of 5–8 days, based on the analysis of the root mean square error (RMSE) of ensemble mean forecast and the local practical predictability limits (Dai et al., 2022; Li et al., 2023). These results suggest that extreme cold events can generally be forecasted accurately with a lead time of about 7 days, after which forecast errors become significantly larger.

Previous studies primarily focus on the average performance of the extreme cold events, but rarely examine the characteristics of forecast error growth over time and the underlying mechanisms driving this growth. If different growth rates occur during the intensification stage and decay stage of extreme cold events, distinct forecast post-processing strategies should be adopted. Although many studies have investigated the formation mechanisms of extreme cold events in China (e.g., Li et al., 2019; Yu et al., 2022; Zuo et al., 2015), they cannot answer these questions. This study will analyze the operational forecasts of extreme cold events from 2008 onwards, excluding a few cases for which data from the International Grand Global Ensemble (TIGGE) are unavailable. The growth patterns of forecast errors will be investigated and summarized, followed by an explanation of the underlying physical mechanisms.

The remainder of this paper is organized as follows: Section 2 describes the data and methods. Section 3 investigates the "predictability barrier" phenomenon and analyzes the underlying mechanisms. Section 4 presents a summary and discussion.

2. Data and Methods Description

The 3-hourly, instantaneous, pressure-level assimilated meteorological fields, temperature (t), zonal wind (u), meridional wind (v), and vertical pressure velocity (ω), along with the hourly surface air temperature at 2m (T_{2m}) are from the Modern-Era Retrospective analysis for Research and Applications, Version 2 (MERRA-2) data (Gelaro et al., 2017; Molod et al., 2015). The daily mean is defined as the average of the data at 00:00, 6:00, 12:00, and 18:00 UTC. The horizontal spatial resolution is 0.5° × 0.625°, and is interpolated to 1.0° × 1.0°. The time period used ranges from 1999 to 2024. The daily climatology is defined as the average over the period from 1999 to 2020, and the anomaly is calculated by subtracting the climatology. Hourly T_{2m} from the fifth generation European Center for Medium Range Forecasting Reanalysis (ERA5) is also used (Hersbach et al., 2023).

The operational forecast products are obtained from the TIGGE data set (Bougeault et al., 2010; Swinbank et al., 2016), accessible through the ECMWF public data sets (https://apps.ecmwf.int/datasets/data/tigge). This study utilizes four products from ECMWF, the China Meteorological Administration (CMA), the Japan Meteorological Agency (JMA) and the National Centers for Environmental Prediction (NCEP). These products contain one control forecast and 30 to 50 perturbed forecasts. The ensemble mean forecast is defined as the average of the control forecast and all perturbed forecasts. The daily mean is derived from the average of the data at 00:00, 6:00, 12:00, and 18:00 UTC. Due to the absence of re-forecast, the MERRA-2 climatology is used to calculate the forecast anomalies.

$$\frac{\partial T'^2}{\partial t} = -\vec{v}_r \cdot \nabla T'^2 + P_B + P_E + P_C + P_Q + P_{\text{residual}} \quad (1)$$

The temperature error budget is described by the above equation: The first term on the right-hand side (rhs) of Equation 1 represents the horizontal transport of temperature error associated with the background flow. $\vec{v}_r$ indicates the horizontal wind in the observation (MERRA-2) and T' indicates the temperature forecast error. The second term on the rhs, denoted as P_B, represents the interaction between the horizontal wind forecast error and the temperature gradient of event itself. The third term, P_E, represents the gain in the temperature error due to the

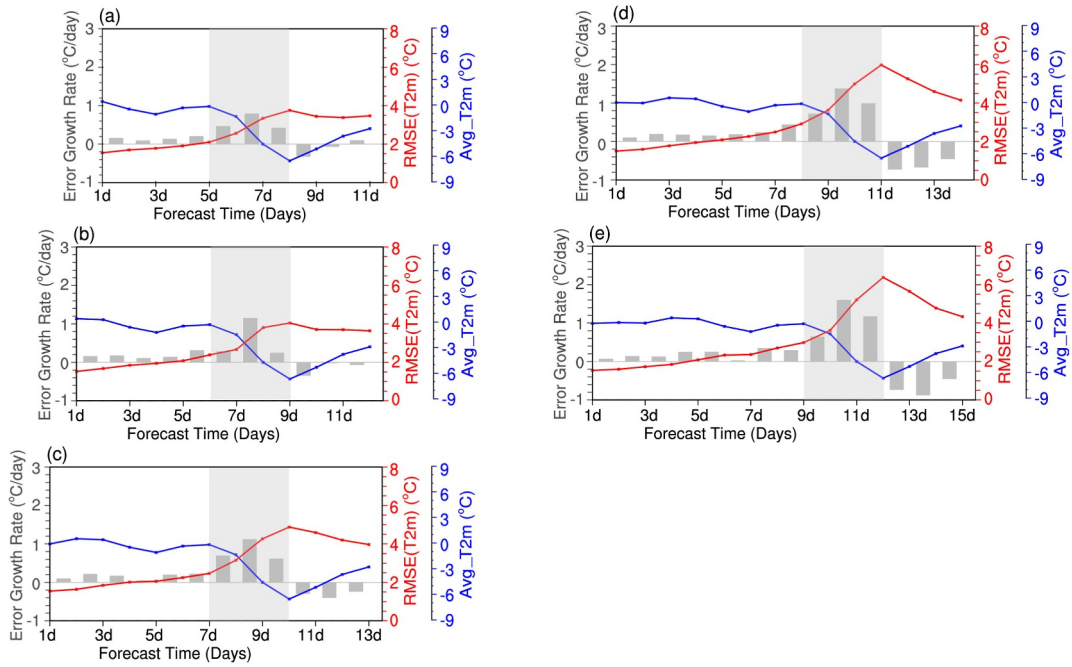

Figure 1. Evolution of the averaged T_{2m} anomaly (blue line, right ordinate with blue color; unit: °C), the averaged root mean square error of T_{2m} ensemble mean forecast (red line, right ordinate with red color; unit: °C), and error growth rate (gray bar, left ordinate; unit: °C/day) over central and eastern China (23°N–40°N, 105°E–123°E). The three indices are the compositions of 15 extreme cold events. (a–e) Indicate the initial times which are 8–12 days prior to the peak day of events. The composition of these indices is centered on the peak day of each extreme cold event. The *x*-axis indicates the forecast time in days. The forecast data is from ECMWF. The gray shading denotes the intensification stage.

interaction between the horizontal wind error and the gradient of temperature error. The fourth term, P_c, corresponds to the conversion from available potential energy (APE) error to kinetic energy error. The fifth term, P_Q, represents the error generation resulting from the adiabatic heating error. The final term, P_{residual}, represents residual errors caused by spatial and temporal discretization. The derivation follows that of the APE equation in Zhuge and Tan (2021), with further details provided in Appendix A.

3. Results

3.1. Extreme Cold Events

The extreme cold events across central and eastern China are first identified. An extreme cold event is defined as follows: if the daily mean of the T_{2m} anomaly over central and eastern China (23°N–40°N, 105°E–123°E) is lower than −1.0 standard deviations for three consecutive days, and the lowest value is less than −2.0 standard deviations, the event is classified as an extreme cold event. The events during December and January, which are the coldest period of the year, are selected. Based on this criterion, a total of 18 events are identified; however, due to the unavailability of forecast data in some instances, only 15 events are ultimately analyzed (see Table S1 in Supporting Information S1). These selected events have been reported in previous research. The peak day of the extreme cold event is defined as the day with the lowest anomaly value, and the peak day of each event is presented in Table S1 of Supporting Information S1. Typically, the T_{2m} anomaly begins to decrease 3 days prior to the peak day, as illustrated by blue lines in Figure 1. Consequently, the 3 days prior to the peak day are defined as the intensification stage. Similarly, the 3 days following the peak day are defined as the decay stage.

3.2. The Phenomenon of "Predictability Barrier"

Figure 1 illustrates the temporal evolution of three metrics over central and eastern China (23°N–40°N, 105°E–123°E), derived from a composite analysis of 15 extreme cold events. The blue lines represent the averaged T_{2m} anomaly (MERRA-2), which describes the temporal evolution of the strength of cold events in central and eastern China and is used to identify extreme cold events in Section 3.1. The red lines represent the averaged RMSE of the

T_{2m} ensemble mean forecast when the initial times are 7–14 days prior to the peak day of events. The gray bars indicate the error growth rate, representing the daily variation in the forecast error. For example, the gray bar on the far left of Figure 1a indicates the difference in forecast error between the 2nd day and the 1st day. Only forecasts with the initial time longer than 7 days prior to the peak of the events are presented, as T_{2m} forecasts are generally accurate at lead times shorter than 7 days, as noted in the introduction.

There are two common characteristics of forecast error growth. First, forecast error exhibits rapid growth during the intensification stage, which is marked by the gray shading in Figure 1, with the growth rate reaching its maximum (gray bars in Figure 1). The magnitude of error growth during this stage varies with different lead times (Figures 1a–1e). This stage accounts for approximately 68%–75% of the error growth from day 1 to the peak day of events, and about 80%–130% of the error growth from day 1 to the third day after the peak. Analogous to the "spring predictability barrier" observed in El Niño-Southern Oscillation (ENSO), which describes the rapid error growth during the spring (e.g., Mu et al., 2007; Webster & Yang, 1992), we identify the phenomenon of the rapid error growth in this study as "predictability barrier" of extreme cold events. Second, forecast error decreases during the decay stage, with the growth rate approaching zero or even becoming negative. The "predictability barrier" becomes more pronounced with increasing lead times (Figures 1a–1e), indicating that the decay stage is forecasted more accurately than the intensification stage with identical lead time. For example, the RMSE on the 11th day in Figure 1e (intensification stage) is 5.16°C, significantly higher than those in Figure 1a (3.38°C), Figure 1b (3.36°C) and Figure 1c (4.53°C) (decay stage). Although RMSE has been analyzed, it remains unclear whether forecast products overestimate or underestimate these events. Therefore, we compare observed and forecasted anomalies. Results indicate a consistent temperature underestimation across all models (Figure S1 in Supporting Information S1), with the underestimate increasing more rapidly during the intensification stage and decreasing during the decay stage, which is similar to the evolution of RMSE.

Individual analyses are conducted for each event to ensure that the composite analysis reflects the common characteristics of all events, rather than being influenced by a few outliers. The results indicate that error growth during the intensification stage (−3d to 0d) is larger than decay stage (0d to 3d) and the period before intensification stage (−6d to −3d), and 0d indicates the peak day. These findings suggest that nearly all cases exhibit characteristics similar to the composite, implying that the "predictability barrier" is a common feature in ECMWF forecasts. Figure 2 only shows the result when the initial time leads the peak day by 7 days. Similar results are obtained when the initial time leads the peak day by more than 7 days (not shown), except that the number of cases with the "predictability barrier" increases. The above analyses are based on the forecast from ECMWF. A pertinent question arises: whether the "predictability barrier" also exists in other operational models? To answer this, the forecasts from CMA, JMA and NCEP are examined, and the selected cases are listed in Table S2 of Supporting Information S1. The results show that the evolution of forecast errors in CMA, JMA and NCEP models display similar characteristics to those in ECMWF (Figure 3). Forecast errors grow rapidly during the intensification stage (warm colors shading during the period from −3 days to 0 day), and decrease during the decay stage (cool colors shading during the period from 0 day to 3 days), and 0d indicates the peak day. The main differences among four models are the magnitudes of error growth rate. To ensure result robustness, forecast errors were further evaluated against ERA5 observational data. The results are in agreement with those obtained using MERRA2 as the validation (Figure S2 in Supporting Information S1).

The "predictability barrier" manifests as a common characteristic in operational forecasts when the initial time prior to the peak day exceeds 7 days. Although the initial condition errors and model errors are the sources of the forecast errors (Lorenz, 1969), the consistent occurrence of this phenomenon across various events and models implies that the inherent physical processes governing event intensification may significantly amplify these errors. As a result, the mechanisms responsible for error amplification are investigated in the following subsection.

3.3. Mechanisms of "Predictability Barrier"

To understand the occurrence of the "predictability barrier," we analyzed the contributions of different physical processes to error amplification. The forecast error of temperature at 850 hPa (T_{850}) is analyzed instead of T_{2m}, since T_{2m} is a diagnostic variable rather than a prognostic one, while T_{850} is a prognostic variable in the physical equations of the atmospheric model. Moreover, T_{850} errors also exhibit a pronounced "predictability barrier" during the intensification stage, and decrease during the decay stage (Figure S3 in Supporting Information S1). The derivation of the temperature error budget equation is given in the Appendix A. The derivation refers to that

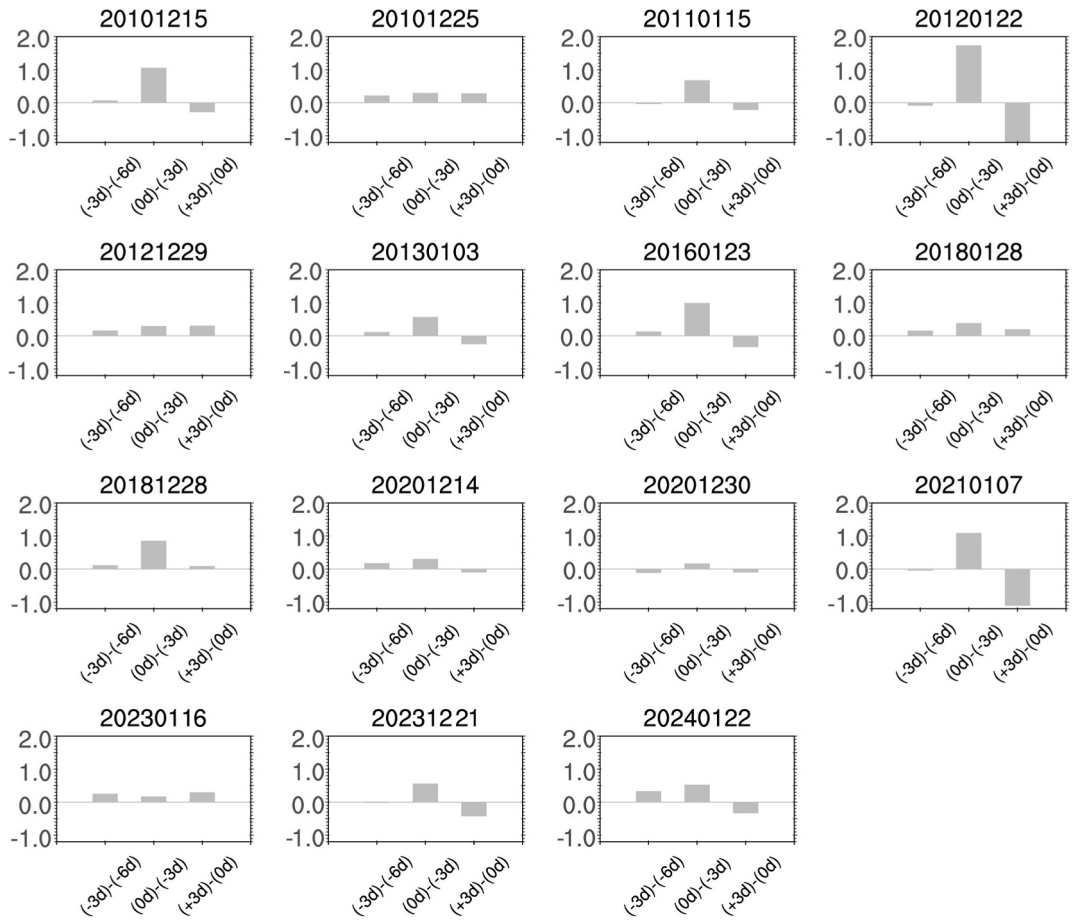

Figure 2. Error growth rate (unit: °C/day) during different stages in 15 cases when the initial time leads the peak day of each event 7 days. The time of the peak day of each event is shown on the top of each panel. (–3d to −6d): the stage before the intensification stage, (0d to −3d): the intensification stage, (+3d–0d): the decay stage. 0d denotes the peak day of events.

of the APE budget equation in Tanaka et al. (2016) and Zhuge and Tan (2021). In fact, the APE is proportional to the square of temperature. Because the diabatic heating can be only calculated indirectly through thermodynamic equation and is influenced by data resolution, it is not analyzed separately in this study. It should be noted that only four events are investigated. This limitation arises from the fact that the vertical velocity for these events can only be obtained from the National Meteorological Center of CMA and is not available from TIGGE. The spatial coverage of these data is 0°N–70°N and 40°E−160°E, and the available forecast period is 10 days.

Figures 4a and 4b illustrate the area-averaged T_{850} error tendency and the conversion terms over central and eastern China (23°N–40°N, 105°E–123°E), derived from a composite of four events. During the intensification stage, the primary source of error growth is the interaction between the horizontal wind forecast error and the horizontal temperature gradient of the event in the observation (P_B). This interaction represents the baroclinic energy conversion from the background flow within the framework of APE theory. The RMSE of horizontal wind at 850 hPa over the study region is analyzed. The results show that the peak in the horizontal wind forecast error precedes the peak of the T_{2m} forecast error by 1 day (Figure S4 in Supporting Information S1), thereby contributing to temperature error growth according to Equation A7. In fact, the horizontal wind forecast error in the P_B term is related to the atmospheric circulations that control the extreme cold events, such as the blocking high extending from Ural to East Asia, the East Asian trough and the Siberian High (e.g., Han et al., 2011; Han & Li, 2020; Li, 2004; Luo et al., 2016; Peng et al., 2021). The terms representing the horizontal transport of errors due to background flow of the event ($-\vec{v}_r \cdot \nabla T'^2$), the interaction from errors themselves (P_E), and the conversion between the kinetic energy and APE error (P_C) all have negative impacts on the error tendency. Among these, the contribution of the P_C term is the largest. The sums of all the conversion terms are generally consistent with the

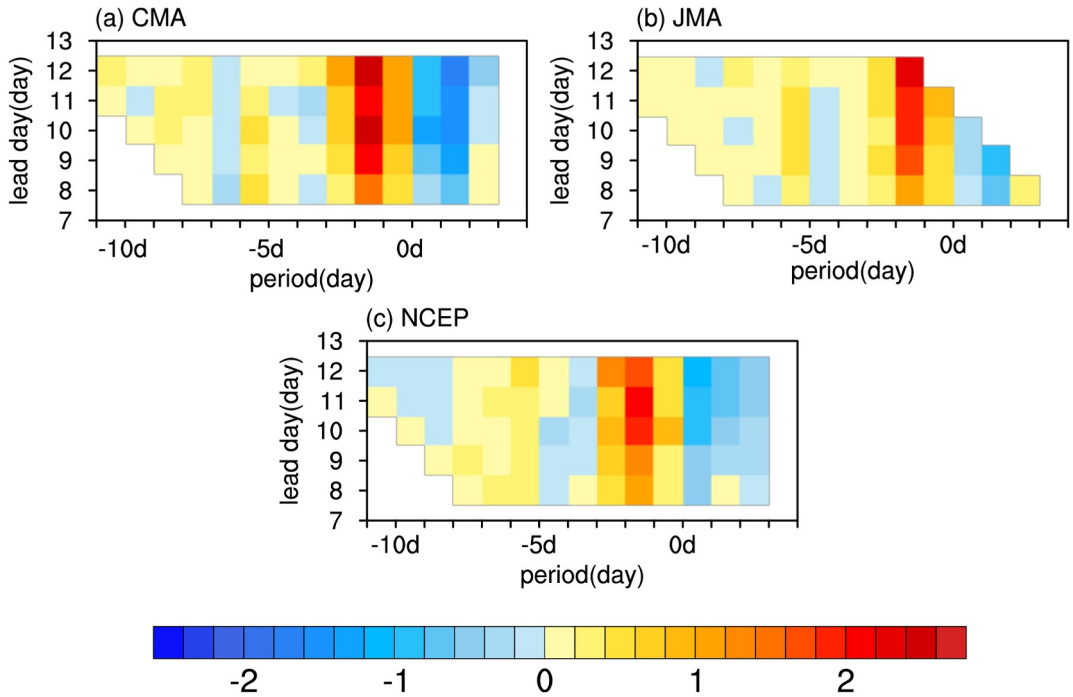

Figure 3. Evolution of error growth rate (units: °C/day) with the forecast from China Meteorological Administration (a), Japan Meteorological Agency (b) and NCEP (c). 0d denotes the peak day of events. Ordinate denotes the days that the initial time leads the peak day.

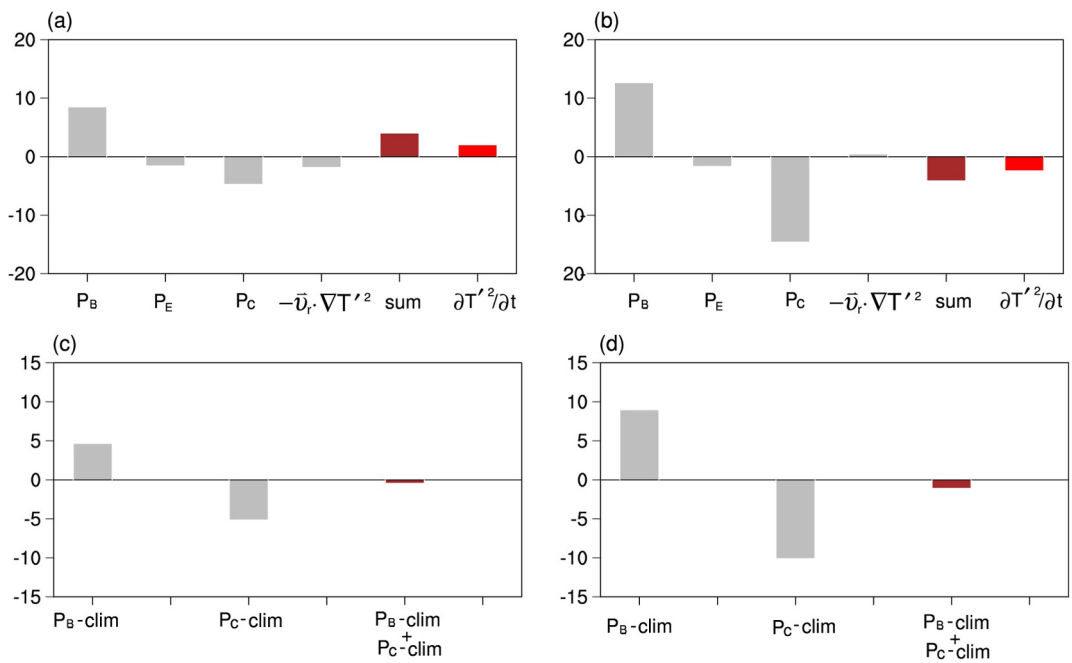

Figure 4. Tendency of temperature error and the generation terms (units: °C/day) for (a) intensification and (b) decay stages of events: P_B, P_E, P_C, $-\vec{v}_r \cdot \nabla T'^2$ (gray bars), the sum of P_B, P_E, P_C, and $-\vec{v}_r \cdot \nabla T'^2$ (brown bar), and tendency of temperature error (red bar); P_B-clim, P_C-clim (gray bars), and their sum (brown bar) for (c) intensification and (d) decay stages. Details of meanings of generation terms are in Section 2 and the Appendix A.

error tendency (brown bars vs. red bars), while the differences between them are from the roles of the diabatic heating error, as well as the horizontal, vertical and time resolution. During the decay stage, the P_C term becomes negative and decreases sharply relative to that in the intensification stage, while the P_B term varies a little. Consequently, the error decrease (i.e., the negative value of the error tendency) is primarily dominated by the P_C term, which is associated with the negative vertical velocity and positive temperature error. Moreover, the difference in the P_C term controls the variation of error tendency between the intensification and decay stages.

To further examine whether the inherent physical processes governing event evolution play the dominant role in the amplification of forecast error, the temperature of the background state (T_r in the P_B term), and σ in the P_C term are substituted by the climatological mean temperature. The contributions from these substitutions are labeled as P_B-clim and P_C-clim, respectively. The combined contribution of P_B-clim and P_C-clim to error growth is negative during the intensification stage of events (Figure 4c). Therefore, the inherent physical processes governing event intensification play a dominant role in the amplification of forecast error through interactions with the initial and model errors. The combined contribution of P_B-clim and P_C-clim to error reduction is positive during the decay stage, accounting for approximately half of the error reduction caused by combined P_B and P_C (Figure 4d). This reveals that error reduction during the decay stage is controlled by the interactions among the inherent physical processes governing event evolution, climatology, and initial and model errors.

4. Conclusions and Discussions

Forecast analyses of 15 extreme cold events in central and eastern China reveal that the forecast errors of ensemble mean T_{2m} exhibit rapid intensification during the intensification stage of these events, reaching the largest error growth rate throughout the entire forecast period. Analogous to the "spring predictability barrier" observed in ENSO forecasting, the rapid growth of T_{2m} forecast error during the intensification stage is defined as the "predictability barrier" of extreme cold events. The "predictability barrier" becomes more pronounced with longer lead times. In contrast, the forecast errors show a slight decrease during the decay stage of these events. These results suggest that the decay stage is more accurately forecasted than the intensification stage when the lead time is same. As a result, different post-processing strategies should be adopted for these stages. Further analyses indicate that all models underestimate the extreme cold events.

The "predictability barrier" is seen in different events and across various operational models, suggesting that this phenomenon may be related to the inherent physical processes governing event evolution. In other words, initial and model errors are amplified by these inherent physical processes during the intensification stage. To elucidate the mechanisms driving error growth, an analysis is conducted using the temperature error budget equation. The results indicate that error growth is predominantly driven by the interaction between the horizontal wind error and the background temperature gradient (P_B term). Because the error amplification during the intensification stage corresponds to the increased underestimation, the mechanisms explaining error amplification can also elucidate the increase of underestimation. Conversely, error reduction is controlled by the energy conversion from APE error to kinetic energy error. Further analysis reveals that the inherent physical processes governing event evolution play a crucial role in driving error amplification during the intensification stage. From this perspective, some summer heatwaves also have a rapid intensification process (Liu et al., 2025), and therefore their enhancement mechanisms may contribute to error amplification and lead to a phenomenon of "predictability barrier", which is an interesting question to investigate. The roles of the horizontal wind and the gradient of temperature in the extreme cold events are actually related to the atmospheric circulations that trigger such events, such as the blocking high, the Siberian High and the East Asian trough. Whether a "predictability barrier" exists in such atmospheric circulation predictions warrants future investigation.

From the perspective of error sources in numerical forecast, there are two types of error sources, the initial error and the model error. In this study, each operational model contains both the initial error and the model error, and their effects cannot be effectively separated by statistical methods. In the future, their relative contribution to the "predictability barrier" and the underestimation needs to be investigated through numerical model experiments.

Appendix A: Derivation of Temperature Error Equations

The temperature error budget equation is derived here, and then used to analyze the evolution of temperature error tendency. The following is the thermodynamic equation in pressure coordinate:

$$\left(\frac{\partial}{\partial t}+u\frac{\partial}{\partial x}+v\frac{\partial}{\partial y}\right)T-\sigma\omega=\frac{\dot{Q}}{C_p} \tag{A1}$$

where u, v, ω, and T are the zonal, meridional, vertical pressure velocities, and air temperature at pressure-level, $\sigma=\frac{RT_r}{pC_p}-\frac{\partial T_r}{\partial p}$ is the static stability parameter, $\dot{Q}$ is the total diabatic heating rate (including the convective, sensible heating rate, longwave and shortwave radiative heating rate). Both the reanalysis data and the forecast data satisfy the temperature equation. Substitution reanalysis data $(u_r, v_r, \omega_r, T_r, \dot{Q}_r)$ into (Equation A1) yields

$$\frac{\partial T_r}{\partial t}+u_r\frac{\partial T_r}{\partial x}+v_r\frac{\partial T_r}{\partial y}-\sigma\omega_r=\frac{\dot{Q}_r}{C_p} \tag{A2}$$

Substituting forecast data $(u_f, v_f, \omega_f, T_f, \dot{Q}_f)$ into (Equation A1) yields

$$\frac{\partial T_f}{\partial t}+u_f\frac{\partial T_f}{\partial x}+v_f\frac{\partial T_f}{\partial y}-\sigma\omega_f=\frac{\dot{Q}_f}{C_p} \tag{A3}$$

The forecast can be separated into the reanalysis (MERRA-2) and the error (primes):

$$u_f=u_r+u', v_f=v_r+v', \omega_f=\omega_r+\omega', T_f=T_r+T' \tag{A4}$$

Substitution of (Equation A4) into (Equation A3) yields

$$\begin{aligned}&\frac{\partial T_r}{\partial t}+\frac{\partial T'}{\partial t}+u_r\frac{\partial T_r}{\partial x}+u_r\frac{\partial T'}{\partial x}+u'\frac{\partial T_r}{\partial x}+u'\frac{\partial T'}{\partial x}+v_r\frac{\partial T_r}{\partial y}+v_r\frac{\partial T'}{\partial y}+v'\frac{\partial T_r}{\partial y}+v'\frac{\partial T'}{\partial y}-\sigma\omega_r-\sigma\omega'\\&=\frac{\dot{Q}_r}{C_p}+\frac{\dot{Q}'}{C_p}+\text{residual}\end{aligned} \tag{A5}$$

Subtracting (Equation A2) from (Equation A5) leads to:

$$\frac{\partial T'}{\partial t}+u_r\frac{\partial T'}{\partial x}+u'\frac{\partial T_r}{\partial x}+u'\frac{\partial T'}{\partial x}+v_r\frac{\partial T'}{\partial y}+v'\frac{\partial T_r}{\partial y}+v'\frac{\partial T'}{\partial y}-\sigma\omega'=\frac{\dot{Q}'}{C_p}+\text{residual} \tag{A6}$$

Multiplying (Equation A6) with T' yields the temperature error budget equation:

$$\frac{\partial T'^2}{\partial t}=-\vec{v}_r\cdot\nabla T'^2+P_B+P_E+P_C+P_Q+P_{\text{residual}} \tag{A7}$$

where

$$P_B=-\frac{RT'}{p\sigma}\left(u'\frac{\partial T_r}{\partial x}+v'\frac{\partial T_r}{\partial y}\right)$$

$$P_E=-\frac{RT'}{p\sigma}\left(u'\frac{\partial T'}{\partial x}+v'\frac{\partial T'}{\partial y}\right)$$

$$P_C=\frac{R}{p\sigma}\omega'T'$$

$$P_Q=\frac{R}{p\sigma}\frac{\dot{Q}'T'}{C_p}$$

If the square of temperature error is multiplied by $\frac{R}{p\sigma}$, it represents the error of APE (see Kosaka & Nakamura, 2006; Zhuge & Tan, 2021). The P_B term represents the interaction between the horizontal wind forecast error and the horizontal temperature gradient of the event in the observation. The P_E term represents the interaction between the horizontal wind error and the gradient of temperature error. The P_C term represents the error generation related to conversion from the APE error to kinetic error. The P_Q term represents the error generation caused by adiabatic heating error. Equation A7 instead of Equation A6 is used to maintain consistency with RMSE analysis. Additionally, positive and negative T' may coexist, and spatial averaging will lead to cancellation and cause an underestimation of error magnitude. To avoid such issue, Equation A7 is employed.

Conflict of Interest

The authors declare no conflicts of interest relevant to this study.

Data Availability Statement

Open access data sets supporting the findings of this study can be found in the following repository: The forecasts from ECMWF, CMA, JMA and NCEP are available in the THORPEX Interactive Grant Global Ensemble (Bougeault et al., 2010; Swinbank et al., 2016) (https://apps.ecmwf.int/datasets/data/tigge). The MERRA-2 reanalysis on single level are from Global modeling and Assimilation Office (GMAO, 2015a), and the MERRA-2 reanalysis on pressure levels are from Global modeling and Assimilation Office (GMAO, 2015b). The vertical velocity forecast can be accessed from Zenodo (Han et al., 2025). T_{2m} from ERA5 are downloaded from Climate Data Store (Hersbach et al., 2023).

Acknowledgments
The authors are grateful to the Editor and the two anonymous reviewers for their helpful comments and suggestions, which have greatly improved this manuscript. This research is sponsored by the National Natural Science Foundation of China (Grant 42288101), the Meteorological Joint Fund (Grant U2442221), the National Natural Science Foundation of China (Grant 42494871, 42475054) and Shanghai Key Laboratory of Ocean-land-atmosphere Boundary Dynamics and Climate Change. We thank for the technical support of the National Large Scientific and Technological Infrastructure "Earth System Numerical Simulation Facility" (https://cstr.cn/31134.02.EL).

References

Bougeault, P., Toth, Z., Bishop, C., Brown, B., Burridge, D., Chen, D. H., et al. (2010). The THORPEX interactive grand global ensemble. *Bulletin of the American Meteorological Society*, *91*(8), 1059–1072. https://doi.org/10.1175/2010bams2853.1

Chen, B., Cui, H., Qiao, F., Zhang, Z. Q., Sun, X. H., Gao, C., & Yang, S. (2024). Causes of the extreme cold event in December 2023 on Eastern China. *Environmental Research Communications*, *6*(1), 081002. https://doi.org/10.1088/2515-7620/ad6bf7

Dai, G., Li, C., Han, Z., Luo, D., & Yao, Y. (2022). The nature and predictability of the East Asian extreme cold events of 2020/21. *Advances in Atmospheric Sciences*, *39*(4), 566–575. https://doi.org/10.1007/s00376-021-1057-3

Dai, G., Mu, M., Li, C., Han, Z., & Wang, L. (2021). Evaluation of the forecast performance for extreme cold events in east Asia with subseasonal-to-seasonal datasets from ECMWF. *Journal of Geophysical Research: Atmospheres*, *126*(1), e2020JD033860. https://doi.org/10.1029/2020jd033860

Dong, W., Zhao, L., Zhou, S. W., & Shen, X. Y. (2020). A synergistic effect of blockings on a persistent strong cold surge in East Asia in January 2018. *Atmosphere*, *11*(2), 215. https://doi.org/10.3390/atmos11020215

Gelaro, R., McCarty, W., Suárez, M. J., Todling, R., Molod, A., Takacs, L., et al. (2017). The modern-era retrospective analysis for research and applications, version 2 (MERRA-2). *Journal of Climate*, *30*(14), 5419–5454. https://doi.org/10.1175/jcli-d-16-0758.1

Global Modeling and Assimilation Office (GMAO). (2015b). MERRA-2 inst3_3d_asm_Np: 3d,3-Hourly,Instantaneous,Pressure-Level,Assimilation,Assimilated meteorological fields V5.12.4, Greenbelt, MD, USA [Dataset]. *Goddard Earth Sciences Data and Information Services Center (GES DISC)*. https://doi.org/10.5067/QBZ6MG944HW0

Global Modeling and Assimilation Office (GMAO). (2015a). MERRA-2 inst1_2d_asm_Nx: 2d,1-Hourly,Instantaneous,Single-Level,Assimilation,Single-Level diagnostics V5.12.4, Greenbelt, MD, USA [Dataset]. *Goddard Earth Sciences Data and Information Services Center (GES DISC)*. https://doi.org/10.5067/3Z173KIE2TPD

Gong, H., Ma, K., Wang, L., & Chen, W. (2024). Attribution of the record-breaking extreme cold event over Northern East Asia in December 2023. *Environmental Research Letters*, *51*(23), e2024GL112568. https://doi.org/10.1029/2024gl112568

Han, Z., Duan, W., Dai, G., Chen, B., Li, S., & Hou, Y. (2025). The "predictability barrier" phenomenon of winter extreme cold events in East China and mechanisms of error amplification [Dataset]. *Zenedo*. https://doi.org/10.5281/zenodo.17479725

Han, Z., & Li, S. L. (2020). Atmospheric responses over Asia to sea ice loss in the Barents and Kara seas in mid–late winter and early spring: A perspective revealed from CMIP5 data. *Adv. Polar. Sci.*, *31*, 55–63.

Han, Z., Li, S. L., & Mu, M. (2011). The role of warm North Atlantic SST in the formation of positive height anomalies over the Ural Mountains during January 2008. *Advances in Atmospheric Sciences*, *28*(2), 246–256. https://doi.org/10.1007/s00376-010-0069-1

Hersbach, H., Bell, B., Berrisford, P., Biavati, G., Horányi, A., Muñoz Sabater, J., et al. (2023). ERA5 hourly data on single levels from 1940 to present [Dataset]. *Copernicus Climate Change Service (C3S) Climate Data Store (CDS)*. https://doi.org/10.24381/cds.adbb2d47

Huang, J. L., Hitchcock, P., Tian, W. S., & Sillin, J. (2022). Stratospheric influence on the development of the 2018 late winter European cold air outbreak. *Journal of Geophysical Research: Atmospheres*, *127*(5), e2021JD035877. https://doi.org/10.1029/2021jd035877

Kosaka, Y., & Nakamura, H. (2006). Structure and dynamics of the summertime Pacific–Japan teleconnection pattern. *Quart. J. Roy. Meteor. Soc.*, *132*(619), 2009–2030. https://doi.org/10.1256/qj.05.204

Lalaurette, F. (2003). Early detection of abnormal weather conditions using a probabilistic extreme forecast index. *Quarterly Journal of the Royal Meteorological Society*, *129*(594), 3037–3057. https://doi.org/10.1256/qj.02.152

Li, S. L. (2004). Impact of Northwest Atlantic SST anomalies on the circulation over the Ural Mountains during early winter. *Journal of the Meteorological Society of Japan*, *82*(4), 971–988. https://doi.org/10.2151/jmsj.2004.971

Li, X., Ding, R. Q., & Li, J. (2023). The BaSIC method: A new approach to quantitatively assessing the local predictability of extreme weather events. *Climate Dynamics*, *60*(11–12), 3561–3576. https://doi.org/10.1007/s00382-022-06526-4

Li, Y., Zhang, J. Y., Lu, Y., Zhu, J. L., & Feng, J. (2019). Characteristics of transient eddy fluxes during blocking highs associated with two cold events in China. *Atmosphere*, *10*(5), 235. https://doi.org/10.3390/atmos10050235

Liu, C., Jiang, Q., & Gui, H. L. (2018). Analysis of the January 2018 atmospheric circulation and weather. *Meteorological Monographs*, *44*, 590–596. (In Chinese).

Liu, H., Sun, G., Mu, M., Zhang, Q., & Chen, B. (2025). Nonlinear synergistic effects of three-dimensional soil moisture errors on uncertainties in subseasonal heatwave onset predictions in the Yangtze River region. *Quart. J. Roy. Meteor. Soc.*, e70079. https://doi.org/10.1002/qj.70079

Lorenz, E. (1969). The predictability of a flow which possesses many scales of motion. *Tellus*, *21*(3), 289–307. https://doi.org/10.3402/tellusa.v21i3.10086

Luo, D., Xiao, Y., Yao, Y., Dai, A., Simmonds, I., & Franzke, C. L. E. (2016). Impact of ural blocking on winter warm Arctic-cold Eurasian anomalies. Part I: Blocking-induced amplification. *Journal of Climate*, *29*(11), 3925–3947. https://doi.org/10.1175/jcli-d-15-0611.1

Ma, S. M., & Zhu, C. W. (2019). Extreme cold wave over East Asia in January 2016: A possible response to the larger internal atmospheric variability induced by Arctic warming. *Journal of Climate*, *32*(4), 1203–1216. https://doi.org/10.1175/jcli-d-18-0234.1

Molod, A., Takacs, L., Suarez, M., & Bacmeister, J. (2015). Developme nt of the GEOS-5 atmospheric general circulation model: Evolution from MERRA to MERRA-2. *Geoscientific Model Development*, *8*(5), 1339–1356. https://doi.org/10.5194/gmd-8-1339-2015

Mu, M., Xu, H., & Duan, W. S. (2007). A kind of initial errors related to "spring predictability barrier" for El Nino event in Zebiak-Cane model. *Geophysical Research Letters*, *34*, L03709. https://doi.org/10.1029/2006GL027412

Peng, J. B., Bueh, C., & Xie, Z. W. (2021). Extensive cold-precipitation-freezing events in southern China and their circulation characteristics. *Advances in Atmospheric Sciences*, *38*(1), 81–97. https://doi.org/10.1007/s00376-020-0117-4

Song, L., & Wu, R. (2017). Processes for occurrence of strong cold events over eastern China. *Journal of Climate*, *30*(22), 9247–9266. https://doi.org/10.1175/jcli-d-16-0857.1

Swinbank, R., Kyouda, M., Buchanan, P., Froude, L., Hamill, T. M., Hewson, T. D., et al. (2016). The TIGGE project and its achievements. *Bulletin of the American Meteorological Society*, *97*(1), 49–67. https://doi.org/10.1175/bams-d-13-00191.1

Tanaka, S., Nishii, K., & Nakamura, H. (2016). Vertical structure and energetics of the western Pacific teleconnection pattern. *Journal of Climate*, *29*(18), 6597–6616. https://doi.org/10.1175/jcli-d-15-0549.1

Tao, Y. W., Dai, K., & Dong, Q. (2017). Extreme analysis and ensemble prediction verification on cold wave process in January 2016. *Meteorological Monographs*, *43*, 1176–1185. (in Chinese).

Webster, P. J., & Yang, S. (1992). Monsoon and ENSO: Selectively interactive systems. *Quarterly Journal of the Royal Meteorological Society*, *118*(507), 877–926. https://doi.org/10.1002/qj.49711850705

Xia, F., & Chen, J. (2012). The research of extreme forecast index based on the T213 ensemble forecast and the experiment in predicting temperature, *38*, 1492–1501. (in Chinese). https://doi.org/10.7519/j.issn.1000-0526.2012.12.006

Yao, Y., Zhang, W. Q., Luo, D. H., Zhong, L. H., & Pei, L. (2022). Seasonal cumulative effect of ural blocking episodes on the frequent cold events in China during the early winter of 2020/21. *Advances in Atmospheric Sciences*, *39*(4), 609–624. https://doi.org/10.1007/s00376-021-1100-4

Ye, Y., Qian, C., Dai, A., Zhang, Y. T., Jiang, J. C., & Zhang, Z. Y. (2025). Attribution of a record-breaking cold event in the historically warmest year of 2023 and assessing future risks. *npj Climate and Atmospheric Science*, *8*(1), 14. https://doi.org/10.1038/s41612-024-00886-w

Yu, Y. Y., Li, Y. F., Ren, R. C., Cai, M., Guan, Z. Y., & Huang, W. (2022). An isentropic mass circulation view on the extreme cold events in 2020/21 winter. *Advances in Atmospheric Sciences*, *39*(4), 643–657. https://doi.org/10.1007/s00376-021-1289-2

Zhang, K., Li, J., Zhu, Z., & Li, T. (2021). Implications from subseasonal prediction skills of the prolonged heavy snow event over Southern China in early 2008. *Advances in Atmospheric Sciences*, *38*(11), 1873–1888. https://doi.org/10.1007/s00376-021-0402-x

Zhang, Y. X., Si, D., Ding, Y. H., Jiang, D. B., Li, Q. Q., & Wang, G. F. (2022). Influence of major stratospheric sudden warming on the unprecedented cold wave in East Asia in January 2021. *Advances in Atmospheric Sciences*, *39*(4), 576–590. https://doi.org/10.1007/s00376-022-1318-9

Zheng, F., Yuan, Y., Ding, Y. H., Li, K. X., Fang, X. H., Zhao, Y. H., et al. (2022). The 2020/21 extremely cold winter in China influenced by the synergistic effect of La Niña and warm Arctic. *Advances in Atmospheric Sciences*, *39*(4), 546–552. https://doi.org/10.1007/s00376-021-1033-y

Zheng, L., Zhang, Y., & Huang, A. (2020). Sub-seasonal prediction of the 2008 extreme snowstorms over South China. *Climate Dynamics*, *55*(7), 1979–1994. https://doi.org/10.1007/s00382-020-05361-9

Zhuge, A., & Tan, B. (2021). The springtime Western Pacific pattern: Its formation and maintenance mechanisms and climate impacts. *Journal of Climate*, *34*(12), 4913–4936. https://doi.org/10.1175/jcli-d-20-0051.1

Zsoter, E. (2006). *Recent developments in extreme weather forecasting* (pp. 8–17). ECMWF Newsletter.

Zuo, Z., Zhang, R., Huang, Y., Xiao, D., & Guo, D. (2015). Extreme cold and warm events over China in wintertime. *International Journal of Climatology*, *35*(12), 3568–3581. https://doi.org/10.1002/joc.4229